Vertical and lateral forces between a permanent magnet and a high-temperature superconductor

John R. Hull and Ahmet Cansiz

Citation: Journal of Applied Physics **86**, 6396 (1999); doi: 10.1063/1.371703
View online: http://dx.doi.org/10.1063/1.371703
View Table of Contents: http://scitation.aip.org/content/aip/journal/jap/86/11?ver=pdfcov
Published by the AIP Publishing

Vertical and lateral forces between a permanent magnet and a high-temperature superconductor

John R. Hull[a] and Ahmet Cansiz
Energy Technology Division, Argonne National Laboratory, Argonne, Illinois 60439

(Received 2 October 1998; accepted for publication 25 August 1999)

The vertical and horizontal forces and associated stiffnesses on a permanent magnet (PM) above a high-temperature superconductor (HTS) were measured during vertical and horizontal traverses in zero-field cooling (ZFC) and in field cooling (FC). In ZFC, the vertical stiffness was greater in the first descent than in the first ascent and second descent, and the stiffness in the second descent was between those of the first descent and the first ascent. At the FC position, the vertical stiffness was two times greater than the lateral stiffness at each height, to within 1% of the vertical stiffness value. The cross stiffness of vertical force with respect to lateral position was positive for FC, but negative for ZFC. Free-spin-down experiments of a PM levitated above a HTS were also performed. These results showed that the coefficient of friction is double valued at frequencies just below the rotor resonance, a result attributed to cross stiffness in the PM/HTS interaction. A frozen-image model was used to calculate the vertical and horizontal forces and stiffnesses, and reasonable agreement with the data occurred for vertical or horizontal movements of the PM less than several mm from the FC position. © *1999 American Institute of Physics*. [S0021-8979(99)03223-5]

I. INTRODUCTION

The interaction between a permanent magnet (PM) and a high-temperature superconductor (HTS) has been a subject of considerable interest for the last decade. Diamagnetic and flux pinning properties of HTSs can be used to achieve passive and stable levitation. Applications of HTSs to flywheel systems[1–4] and magnetic bearing systems[5–7] are based on the high pinning forces between HTSs and PMs, which are essential for lateral stability, as explained qualitatively by Brandt.[8] Magnetic stiffness between a PM and a HTS was first measured by Moon *et al*.[9,10] Use in applications has been accompanied by theoretical estimations, together with experimental measurements of the forces and associated stiffnesses on the PM-HTS systems.[11–14] These applications were also advanced by studies of force creep (or drift),[15,16] and the resonance characteristics and nonlinear properties such as cross stiffness.[17,18]

In this article, we describe investigations of both vertical and lateral force components, including their respective stiffnesses in different cooling conditions. We also compare our experimental results with an analytical calculation of forces and respective stiffnesses that is based on a frozen-image method introduced by Kordyuk.[19] In Sec. II, we describe the experimental setup and procedure, and in Sec. III, we show the experimental results. We discuss the experimental and theoretical results in Sec. IV and present the conclusions in Sec. V.

II. EXPERIMENTAL PROCEDURE

A. Force measurements

The experimental apparatus consisted of a cylindrical NdFeB PM attached to an x- and z-axis strain-gauge force transducer, mounted on hand-controlled micrometer stages that provide vertical (z) and horizontal (x) movement at low velocity over an HTS. The PM disk was 12.7 mm in both diameter and thickness and was polarized axially with a magnetization of $\mu_0 M = 0.831$ T. A 6.5-mm-high, 12.7-mm-diam steel keeper immediately above the PM was mechanically connected to the force transducer. Two bulk YBaCuO HTSs were used: each was ≈30 mm in diameter and 12 mm in thickness. The bulk HTSs were melt textured and single domain, with critical temperatures above 90 K and critical current densities estimated from 1 to 4×10^4 A/cm^2 at a temperature of 77 K and in magnetic fields up to 2 kG.

The experiment was performed by first placing the PM at some cooling height (CH) above and approximately over the center of the HTS, with the height measured between the bottom surface of the PM and the top surface of the HTS. The HTS, which was fixed inside an open-topped Styrofoam container, was then cooled by adding liquid nitrogen to the container until the HTS was submerged in the liquid. After boiling around the HTS had subsided for several minutes, indicating thermal equilibrium at 77 K, a series of translational movements of the PM was initiated, and the forces were recorded at each measurement height (MH) or horizontal displacement. The HTS remained submerged in the liquid nitrogen throughout the experiment by adding additional liquid nitrogen to the container as needed. Position of the PM was determined by reading the micrometer stages.

In all of the experiments, the only variation in HTS performance was a small difference in force under identical traverse histories. Qualitatively, the results were identical for both HTSs. The force and stiffness measurements were performed in zero-field cooling (ZFC) and in field cooling (FC). In ZFC, the HTS was cooled below its critical temperature in a magnetic field several orders of magnitude lower than the

[a]Electronic mail: jhull@anl.gov

field at the closest approach of the magnet. In FC, the HTS was cooled below its critical temperature while there was a substantial magnetic field in the vicinity of the HTS. In discussing the results, we will give special attention to the field cooling position (FC_0), in which MH=CH and there is no horizontal displacement.

With our procedure for the force measurement, the closest distance between the PM and HTS was ≈0.5 mm, because if the distance was less than this, the PM would touch the liquid nitrogen. The PM would then cool and its magnetization change significantly, with a resulting reduction in levitation force. More importantly, the liquid nitrogen can form a liquid film between the HTS and the PM, and the surface tension of the film creates a substantial attractive force.

If unregulated, the PM temperature can vary from −10 to −70 °C, even at distances >1 mm from the liquid nitrogen. Because the PM magnetization is temperature dependent, such a variation can significantly change the magnetic field seen by the HTS and obfuscate the force measurement. While the exact temperature dependence will vary with precise composition and manufacturing technique of NdFeB and are seldom reported in the literature for the temperature range of our experiments, an order of magnitude estimate of the dependence may be made from the data presented by Durst and Kronmuller,[20] who show an increase in remanent magnetization of 1.9 mT for each degree K decrease in temperature. This is consistent with the manufacturer's value of −0.11%/K in the temperature range 20 to 100 °C.[21] Because the force in a diamagnetic system is proportional to the square of the magnetization, the force will change by ≈0.4% for each degree of temperature change of the PM.

To prevent large temperature fluctuations, we installed a bifilar winding with a nichrome resistance wire around the PM to keep the PM temperature at about 10 °C, as measured by a thermocouple attached to the side of the PM near its bottom surface. With this kind of winding, the magnetic field produced from this wire was ≈10 G, which was negligible compared to the field from the PM. Because the HTS is always bathed in liquid nitrogen, its temperature does not change.

B. Spin-down measurements

The experiment to measure rotational losses consisted of levitating a NdFeB PM disk rotor over a bulk HTS in a vacuum chamber, with an oil-diffusion pump reducing the pressure to $<10^{-6}$ Torr.[1] The HTS was inside a room-pressure cryochamber, through which liquid nitrogen flowed from a gravity feed at ≈3 kPa. The cryochamber walls and top were electrically insulating fiberglass to avoid eddy-current losses while the PM was rotating. The cryochamber was covered on the top and sides with three thin layers of aluminized Mylar to reduce radiation heat input. Before cooling the HTS, the PM was held by a thin flat plate that was movable in the z (vertical) direction and rotatable around its support post.

Following HTS cool down and positioning of the PM rotor, the support plate was moved away from the rotor to prevent interference during the spin tests. The PM rotation was accelerated and decelerated by a cold gaseous nitrogen jet impinging approximately tangentially on the PM perimeter from a small-diameter copper tube. The nitrogen gas, supplied from a pressurized bottle through a regulator, was cooled by passing it through a heat exchanger submerged in liquid nitrogen before it entered the vacuum chamber; this averted a possible temperature rise in the HTS. Such a temperature rise would decrease the critical current density (J_c) and possibly decrease the levitation height. Once the PM reached the desired speed, the gas jet was shut off. The rotation of the PM was continuously monitored by a tachometer. To obtain good statistics, the PM was allowed to freely spin down for 3–5 min after acceleration, and speeds were recorded at 5 s intervals. When we were interested in details of resonance behavior, we recorded the data every second. Linear regression was used on the data from the free-spin period to calculate the slope of the rotational frequency versus time function (df/dt), which in turn was used to calculate the coefficient of friction.[1] The height of the levitated PM was measured with a traveling telescope at intervals throughout the experiment, and no change in height from the initial levitation value was observed to within 10 μm.

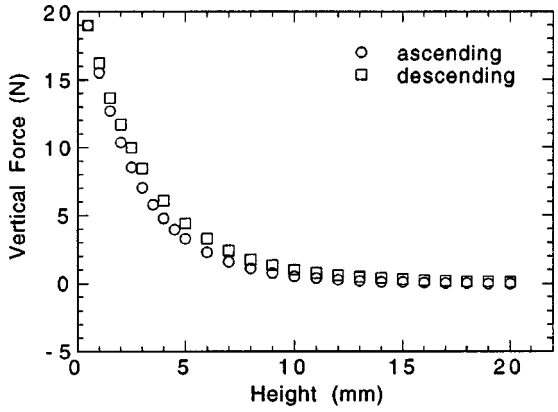

FIG. 1. Vertical force vs height for HTS sample 107 and cooling height CH=30 mm.

III. EXPERIMENTAL RESULTS

A. Forces

Vertical force versus vertical distance has been measured by many researchers (see, for example, Refs. 10 and 22), and the force behavior we have observed was typical of single-domain melt-textured YBaCuO. The HTS was cooled with CH=30 mm (i.e., ZFC), and then vertical force versus vertical distance was measured, as shown in Fig. 1, with a descending vertical traverse to 1 mm, followed by an ascending vertical traverse to 30 mm. Assuming the usual exponential dependence of force on gap, the last several data points in the descending curve near the HTS were extrapolated to find the zero-distance levitation force. Maximum levitation force is 22.4 N, with a corresponding levitation pressure of 177 kPa. The path difference between descending and ascending showed a small hysteresis in the HTS, indicating that the HTS would behave mostly as a diamagnet at this CH, an observation that helped to interpret some of the later

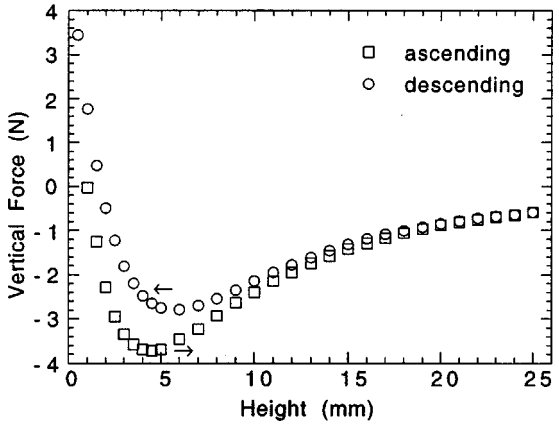

FIG. 2. Vertical force vs height for HTS sample 297 and cooling height CH=0.5 mm.

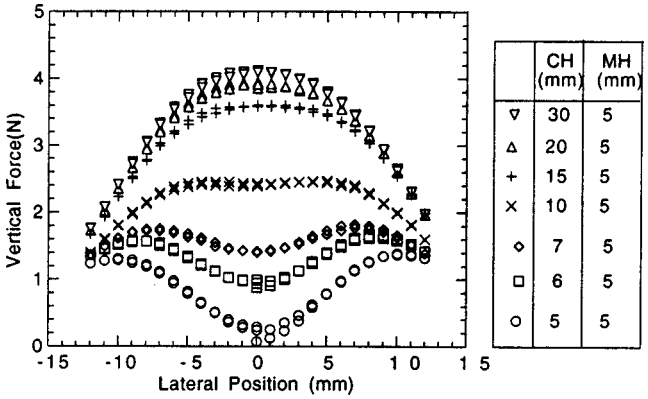

FIG. 3. Vertical force vs lateral position for HTS sample 107 at measurement height MH=5 mm for various cooling height CHs.

measurements when horizontal traverses were performed. Nearly pure diamagnetic behavior is typical of good melt-textured YBaCuO in ZFC. In this series of experiments, the first ascent was often followed by a second descent to 1 mm, and then by a second ascent to 30 mm. In all the samples with CH=30 mm, the force at a given height during the first descent was always greater than the force during the second, whereas the forces during the second ascent were identical to those in the first ascent. This typical behavior[10,22] is qualitatively explained by the well-established critical-state model.

The HTS was again cooled with CH=0.5 mm (i.e., FC), and the vertical force versus vertical distance was measured during an ascending traverse out to 25 mm, followed by a descent to 0.5 mm, as seen in Fig. 2. Compared to that in Fig. 1, the hysteresis loop is much larger in Fig. 2, indicating that flux pinning should play a more dominant role when the CH is lower. This would be expected, even if J_c were independent of magnetic field and flux pinning was equally strong for all PM heights. When only vertical traverses were involved, e.g., as in Figs. 1 and 2, the measured horizontal forces were negligible.

In a second series of measurements, the HTS was cooled with the PM at a given CH, then the PM was moved vertically to a given MH, after which the vertical and horizontal forces were measured in several horizontal traverses. The results for a common MH=5 mm and a horizontal traverse from $x=0$ to $x=12$ mm, followed by a horizontal traverse to $x=-12$ mm, followed by a horizontal traverse to $x=0$ mm, are shown in Figs. 3 and 4. Figure 3 shows the vertical force, and Fig. 4 shows the horizontal force for the same set of measurements. The behavior for CH close to MH is consistent with measurements made by Sugiura *et al.*[18]

The measurements at large CH showed new behavior. As shown in Fig. 3, at large CH (>15 mm), when the magnet moved laterally relative to the center of the superconductor, the vertical force started to decrease because of the edge effect of the HTS (finite size of the HTS). This is consistent with the HTS behaving as a diamagnet. Contrarily, for small CH (≤7 mm) close to MH, when the magnet moved laterally relative to the center of the HTS, the vertical force started to increase. Physically, this results from the interaction of the PM with both the trapped flux at $x=0$ and the diamagnetic image at the new x.

As shown in Fig. 4, at large CH (>15 mm) when the PM moved away from the center of the HTS, the lateral force increased, indicating repulsive force, i.e., the HTS pushed the PM to the side. This behavior can also be observed between two PMs with opposite poles facing each other and is consistent with the HTS behaving as a diamagnet. On the other hand, at small CH (≤7 mm) close to MH, when the PM moved laterally relative to the center of the HTS, the lateral force increased from zero but was then attractive, so the HTS pulled the PM toward its original position. Such behavior results in levitational stability. The transition from large CH to small CH showed that the cooling history determined the HTS behavior. From the data shown in Figs. 3 and 4, the width of the maximum hysteresis in the vertical force was ≈0.04 N, while in the lateral force case it was 0.10 N, indicating that more hysteresis was observed in the lateral force measurement. This result may be attributed to the movement of the flux lines in the HTS, which are mostly in the lateral rather than vertical direction.

B. Stiffness

As an additional and more detailed experimental approach to the studies on force and stiffness measurements

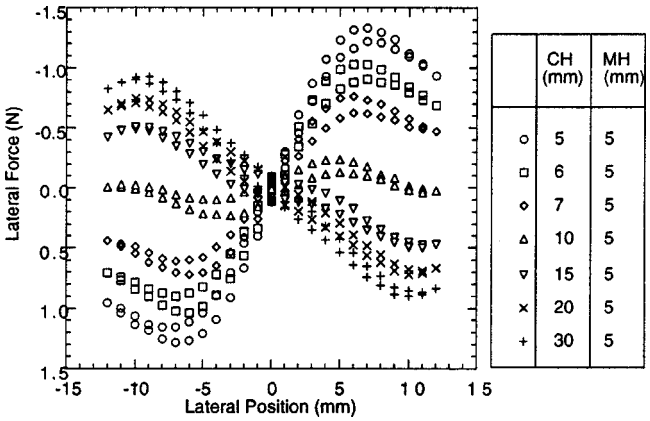

FIG. 4. Lateral force vs lateral position for HTS sample 107 at measurement height MH=5 mm for various cooling height CHs.

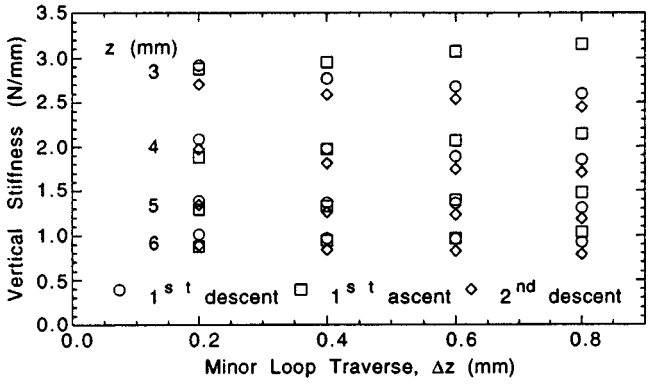

FIG. 5. Vertical stiffness vs minor loop traverse Δz for measurement heights z of 3, 4, 5, and 6 mm for first descent, first ascent, and second descent in ZFC: first descent (circles), first ascent (squares), second descent (diamonds).

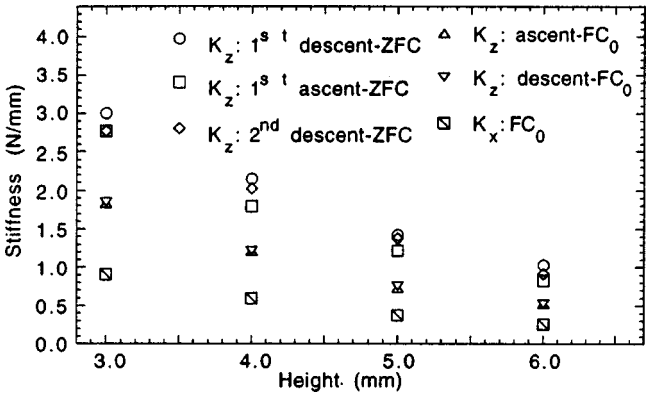

FIG. 6. Stiffness vs height: vertical stiffness first descent (circles), first ascent (squares), and second ascent (diamonds) in ZFC; vertical stiffness for ascending (triangle) and descending (flipped triangle) in FC; and lateral stiffness (squares with diagonal lines) in FC.

reported previously (e.g., Refs. 11–14 and 23), we report the results of stiffness experiments that include vertical stiffness as a function of the descent and ascent height of the PM in ZFC, the relationship between the vertical and lateral stiffness at FC_0, the comparison of the behavior of the vertical stiffness in ZFC and FC_0, the cross stiffness in ZFC and FC, and dependence of the vertical stiffness on path history.

We first measured the average vertical stiffness as a function of vertical distance during the descent and ascent of the PM in ZFC. The HTS was cooled at 30 mm (ZFC) and the stiffness values were determined at heights of 6.0, 5.0, 4.0, and 3.0 mm during the first descent down to 1.0 mm. Upon reversal from 1.0 mm, stiffness values were determined at the same heights for the first ascent; after another reversal at 30 mm, stiffnesses were determined at the same heights for the second descent. In a second series of experiments, we first field cooled at a given height and then immediately measured either the vertical stiffness moving toward the HTS, the vertical stiffness moving away from the HTS, or the lateral stiffness at the FC_0 height. We measured these three stiffnesses at FC_0 heights of 6.0, 5.0, 4.0, and 3.0 mm.

The vertical stiffness values were determined by producing minor hysteresis loops at certain heights, first moving in the opposite direction of the major loop from this height with a small increment and then returning to the same height while the force versus position was measured at the same time. For each height, a series of minor loops were performed with minor loop traverses (Δz) varying from 0.2 to 0.8 mm. Data were taken at every 0.05 mm movement in the vertical direction. All the points of a minor loop were fitted with a straight line to find the slope of each minor loop, which in turn provides the stiffness for a particular Δz. As shown in Fig. 5, the stiffness varied monotonically with Δz, increasing with Δz during ascents and decreasing with Δz during descents. Using linear extrapolation, we found the stiffness at $\Delta z=0$ in the stiffness versus Δz plot (Fig. 5) for each measurement height (3, 4, 5, and 6 mm). This method of extrapolating to zero traverse was followed to find the stiffness value for each stiffness measurement. In the lateral stiffness case, because the measured forces were very small compared to the sensitivity of our experimental setup, the traverses of the minor loops were $\Delta x=0.4$–0.8 mm with a measurement increment of 0.1 mm in the lateral (x) direction.

Stiffnesses for the HTS are plotted in Fig. 6. To a first approximation, the results show that for a given height in ZFC, the vertical stiffness was independent of the ascent or descent, consistent with earlier work.[23] On closer inspection, the vertical stiffness is always slightly greater in the first descent than in the first ascent and second descent, and the stiffness in the second descent is between that of the first descent and the first ascent in ZFC. We attribute these slight differences to different amounts of trapped flux in the HTS. At any point in the HTS, the total applied magnetic field, which is the sum of the field from the PM, the field from the shielding currents producing the diamagnetic image, and the field from the trapped flux in the rest of the HTS, will be greater as the trapped flux increases. In these YBaCuOs, J_c decreases with increasing magnetic field. One thus expects the stiffness to decrease with trapped flux, which is consistent with our measurements. If these stiffness measurements were performed on an HTS where J_c increases with magnetic field, we expect our observed trend in the stiffnesses to reverse.

From the results shown in Fig. 6, for all the heights, at FC_0 the ratio $K_z/K_x=2.02\pm0.02$. In addition, for each height the vertical stiffness was higher in ZFC than for FC_0. These results are predicted by the frozen-flux model, as will be discussed in Sec. IV.

We briefly explored the dependence of vertical stiffness on traverse history. In this experiment, the HTS was cooled with CH=30 mm and $x=0$. In the first case, the PM descended vertically to a height of MH=3 mm above the HTS and then moved laterally from $x=0$ to $x=6$ mm. In the second case, the HTS was again cooled with CH=30 mm and $x=0$. It was then moved laterally to $x=6$ mm, followed by a vertical descent to MH=3 mm and then a lateral traverse from $x=6$ mm to $x=0$. In both cases, vertical stiffness was determined at various locations along the final horizontal traverse, with vertical $\Delta z=0.35$ mm. The stiffnesses are plotted in Fig. 7 and show a slight dependence on path history.

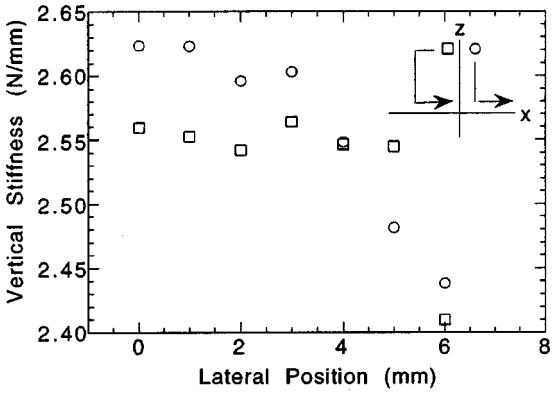

FIG. 7. Vertical stiffness vs lateral position for two traverse paths.

C. Coefficient of friction

Cross stiffness K_{zx}, in which a horizontal displacement results in a change in the vertical force, is evident in the results shown in Fig. 3. The existence of K_{zx} has been shown theoretically to lead to a double-valued function for the radial amplitude of a levitated PM near the radial resonance.[18] This double-valued behavior was seen experimentally, as shown in Fig. 8, which plots the coefficient of friction versus rotational speed. In one set of data (squares), the PM was accelerated to a speed just below the resonant frequency of 5.6 Hz and allowed to freely spin down. In a second set of data (circles), the rotor was accelerated to a speed well above that of the resonance and allowed to spin down. The coefficient of friction is clearly double valued in the frequency range from 5.35 to 5.55 Hz, just below the resonant frequency. The coefficient of friction is significantly higher on the branch that begins above the resonance. Sugiura's *et al*. theory predicts that a higher radial amplitude should exist on the upper branch (i.e., spinning down from above the resonance).[18] A higher amplitude results in a larger hysteresis loss in the HTS, which implies the higher coefficient of friction observed in Fig. 8.

IV. DISCUSSION

Forces on a PM from an HTS are primarily determined by the diamagnetism and flux pinning in the HTS. While diamagnetism provides vertical stability, flux pinning provides the physical basis for suspension and the lateral restoring forces (lateral stability). In particular, flux pinning is dominant in FC, and diamagnetism is dominant in ZFC. In order to analyze the levitation force, many models have been proposed, such as the magnetization model by Brandt,[8] and by Hull *et al*.,[24] the Maxwell-stress tensor model by Moon,[25] and various calculations based on the critical-state model (see Ref. 26 for brief review).

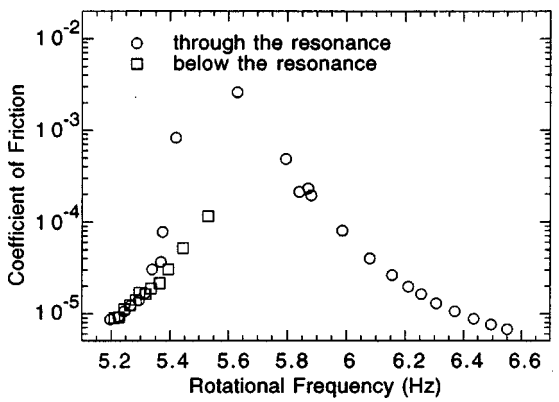

FIG. 8. Coefficient of friction vs rotational frequency through resonance and below resonance.

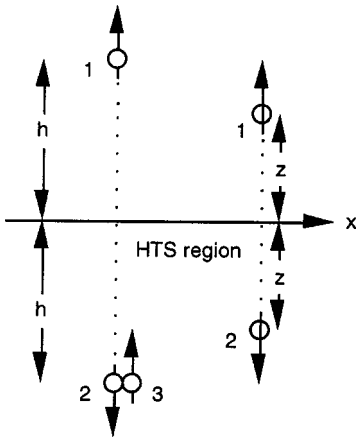

FIG. 9. Schematic diagram of frozen-image method: 1=PM, 2=diamagnetic image, 3=frozen image, z=MH, h=CH.

To describe the PM/HTS interaction in ZFC and FC, we applied the frozen-image method.[19] An attractiveness of this model is that there are no free parameters. The forces may be derived from measured properties of the permanent magnet. The frozen-image model is not expected to be useful in situations where hysteresis effects are significant, but should be useful in many practical applications, such as the calculation of forces and stiffnesses for bearing designs in which melt-textured HTSs are used.

A. Dipole/dipole forces

For a first-order approximation, the PM/HTS interaction can be represented by the forces between dipole images. This approximation readily shows the basic concept of the frozen-image model and produces readily derived analytical expressions. Calculation of forces in realistic geometries requires numerical integration over three dimensions in the most general case and is less practical than the coil/coil calculation presented below. However, the analytical expressions can be used to compare ratios of stiffnesses under various conditions, and these can be compared with the data.

In ZFC, the PM produces its diamagnetic mirror image below the HTS top surface, while in FC, two images appear: one is the diamagnetic mirror image and the other is the frozen image, as illustrated in Fig. 9. The interaction force between PM and HTS is provided by the superposition of the magnetic field from the PM, the source of the frozen image (due to trapped flux in the HTS), and the diamagnetic mirror image (due to screening currents in the HTS). The diamagnetic mirror image moves when the PM moves so that its lateral position equals that of the PM and its vertical height below the HTS surface equals the height of the PM above the

surface. Once formed, the frozen image does not move, and has coordinates $(0,-h)$. The magnitude of the magnetic moment of the frozen image is exactly equal to that of the PM so that there is no net force upon field cooling. This is the typical case with good melt-textured HTSs, such as those that we are using, in which the Meissner fraction after field cooling is negligibly small.

From magnetomechanics, the force between two magnetic dipoles is given as

$$F=(m\cdot\nabla)B, \tag{1}$$

where m is the magnetic moment of one dipole and B is the magnetic field distribution from the other dipole. Solving Eq. (1) using a dipole approximation for the system shown in Fig. 9, the force on a dipole of magnetic moment m_1 at coordinate (x,z) due to a frozen-image dipole of magnetic moment m_2 at coordinates $(0,-h)$ and a diamagnetic-image dipole of moment m_2 at coordinates $(x,-z)$ is

$$F(x,z)=A\left\{\frac{x^3-4x(z+h)^2}{[x^2+(z+h)^2]^{7/2}}\,\hat{x}+\left[\frac{2}{(2z)^4}+\frac{3(z+h)x^2-2(z+h)^3}{[x^2+(z+h)^2]^{7/2}}\right]\hat{z}\right\}, \tag{2}$$

where $A=(3\mu_0 m_1 m_2)/4\pi$, $\hat{x}$ and $\hat{z}$ are unit vectors in the coordinate directions, and h represents the cooling height (CH).

The frozen-image model does not account for flux flow, which would result in a transfer of part of the moment of the diamagnetic image into a small frozen-flux moment as the PM moves. Thus, we do not expect the model to quantitatively predict forces measured in PM/HTS interactions. Nevertheless, when we applied the frozen-image method of Eq. (2) to estimate the vertical force versus distance for a given CH, we found qualitative consistency with the force/distance relations in Figs. 1 and 2. The frozen-image model can also be used to provide a qualitative understanding of the forces produced in lateral motions after FC, similar to the measurements shown in Figs. 3 and 4. The trends are the same for the model and the experimental results. Note that the model does not predict hysteresis in these forces, whereas a small amount of hysteresis is found in the experimental results.

The frozen-image model is more likely to be applicable in FC when the distances moved are small, e.g., in the calculation of stiffnesses near FC_0. In ZFC there is no frozen image, and the diamagnetic mirror image always follows the PM. Thus, in this model there is only a vertical force. Setting h=infinity in Eq. (2),

$$K_z(0,z)=-\frac{\partial F_z}{\partial z}=16\frac{A}{(2z)^5}. \tag{3}$$

At FC_0, in which MH=CH, the lateral and vertical magnetomechanical stiffnesses are found from Eq. (2) respectively, as

$$K_x(0,z)=-\lim_{h\to z}\frac{\partial F_x}{\partial x}=4\frac{A}{(2z)^5}, \tag{4}$$

$$K_z(0,z)=-\lim_{h\to z}\frac{\partial F_z}{\partial z}=8\frac{A}{(2z)^5}. \tag{5}$$

In comparing Eqs. (4) and (5), we see that the model predicts that at FC_0 the vertical stiffness should be exactly twice the lateral stiffness. This is in total agreement with the experimental results shown in Fig. 6 at all heights.

In comparing Eqs. (3) and (5), we see that the model predicts that the vertical stiffness in ZFC should be exactly twice the vertical stiffness at FC_0. In order to make a reasonable comparison between predictions of the frozen-image model and the experimental results for K_z(ZFC) and $K_z(FC_0)$, we must discern whether the measurements in these two cases stay in the region where the HTS behaves as a diamagnet. As can be seen from Fig. 6, for the $K_z(FC_0)$ measurements the maximum deviation from the CH is 0.8 mm, and we always take the limit as Δz goes to zero to determine the actual value. Therefore, the frozen-image model and experimental results are expected to agree with each other. On the other hand, for ZFC the total movement distance is more than 20 mm from the cooling height [i.e., in Fig. 1, the major loop starts from very far away (>20 mm) and ends at 1 mm]. The measurement of K_z(ZFC) was done at certain measurement points along the major loop. As can be seen from Fig. 6, the ratio $K_z(\mathrm{ZFC})/K_z(FC_0)$ is exactly 2 at the measurement point of 6 mm on the major loop, indicating that the HTS behaves as a diamagnet on initial descent for heights of 6 mm and greater. For heights less than 6 mm, the ratio $K_z(\mathrm{ZFC})/K_z(FC_0)$ begins to decrease as the height decreases, reaching a value of 1.62 at a height of 3 mm. The HTS no longer behaves as a diamagnet at heights less than 6 mm because of flux flow in this region. A similar division of domains where flux flow was significant or negligible was found in the vertical forces, as discussed in Sec. IV B below.

If we solve Eq. (2) for cross stiffness, we find

$$K_{zx}(x,z)=\frac{\partial F_z}{\partial x}=\frac{5x(z+h)[4(z+h)^2-3x^2]}{[x^2+(z+h)^2]^{9/2}}A, \tag{6}$$

which predicts a zero cross stiffness at $x=0$, and that cross stiffness decreases with increasing CH, which was observed experimentally.

B. Coil/coil forces

For practical calculations of PM/HTS forces in cylindrical geometries, we find it convenient to model the PM and its images by equivalent Amperian current loops. The forces are represented in terms of complete elliptic integrals, for which polynomial approximations exist.[27] In the most general case, a two-dimensional numerical integration is required, however, if there is no horizontal offset the calculation reduces to a one-dimensional numerical integration.

In the axisymmetric case, i.e., with no horizontal displacement, the axial force F_z between two coaxial current loops is given by[28]

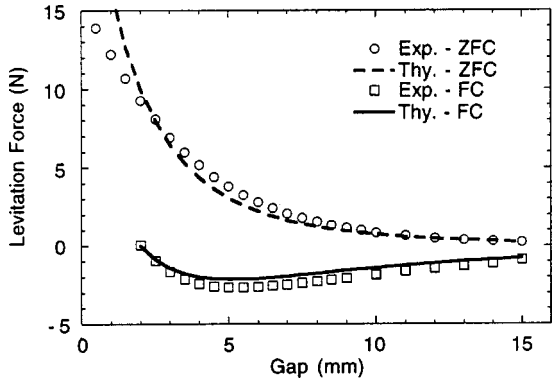

FIG. 10. Comparison of theoretical calculations with experimental values of vertical force vs vertical distance for ZFC and FC.

$$F_z(I_1,I_2,z)=\frac{\mu_0 I_1 I_2 z}{[(R_1+R_2)^2+z^2]^{1/2}} \times\left[-K(k)+\frac{R_1^2+R_2^2+z^2}{(R_1-R_2)^2+z^2}E(k)\right], \quad (7)$$

where $\mu_0=4\pi\times10^{-7}$ N/A^2 is the magnetic permeability of vacuum, I_1 is the current in the first loop of radius R_1, I_2 is the current in the second loop of radius R_2, z is the separation distance between the coils, K is a complete elliptic integral of the first kind, E is a complete elliptic integral of the second kind, and

$$k=\frac{4R_1R_2}{(R_1+R_2)^2+z^2}. \quad (8)$$

The magnetic moments are determined experimentally. First, the PM is rotated at a known speed at the center of a Helmholtz coil and the voltage of the coil measured. The process is repeated with the steel keeper attached. The magnetization of the PM used in our experiments was 661 kA/m and that of the steel keeper was 267 kA/m.

To perform the force calculation, the permanent magnet and its steel keeper are divided into sublayers, and an Amperian current $I_{\mathrm{PM},i}$ assigned to each sublayer i, according to the surface current density determined experimentally. Each sublayer i is assigned a height $z_{\mathrm{PM},i}$ above the HTS surface, calculated from the middle of the sublayer. The diamagnetic and frozen images are similarly subdivided and are denoted respectively by subscripts dia and fr. The total vertical force is given by

$$F_{z,\mathrm{tot}}(z)=\sum_i\sum_j F_z(I_{\mathrm{PM},i},I_{\mathrm{dia},j},z_{\mathrm{PM},i}+z_{\mathrm{dia},j}) +\sum_i\sum_j F_z(I_{\mathrm{PM},i},I_{\mathrm{fr},j},z_{\mathrm{PM},i}+z_{\mathrm{fr},j}). \quad (9)$$

For the numerical calculations we assume that the magnetization of the PM is uniform and divide the PM into 50 identical horizontal sublayers. The steel keeper is similarly divided into 25 horizontal sublayers.

Figure 10 shows a comparison between the theoretical predictions, calculated according to Eq. (9) and experimental results for both ZFC and FC conditions. Considering that there are no free parameters in the theory, the agreement is reasonable. Of course, once the change in magnetic field becomes strong enough that flux begins to penetrate and hysteresis becomes important, the theory is no longer expected to represent the phenomena. This is shown in Fig. 10, where the measured value of vertical force is not well predicted by the frozen-image model in ZFC for heights less than 6 mm and in FC for heights greater than 4 mm. We attribute this lack of agreement to irreversible magnetization in ZFC, as in the critical-state model, with a change of some of the diamagnetic magnetization into trapped-flux magnetization. For ZFC, the domain in which the model appears valid is identical to that for the stiffness measurements, discussed in Sec. IV A above.

The domain where flux flow becomes noticeable for vertical motion of the PM is qualitatively experienced by attempts to stably levitate a free PM over the HTSs used in the measurements, and the results are consistent with the discussion above. In ZFC, if one brings a PM by hand into close proximity with the HTS and then releases it, for heights greater than about 5 mm, the magnet is horizontally unstable and quickly moves into the liquid nitrogen, whereas for release heights less than about 5 mm, the PM will find a stable equilibrium. In FC, the PM will find a stable equilibrium for release heights less than about 10 mm.

It is well known that PMs may have considerable inhomogeneity in their magnetization. One of the more confounding aspects of the inhomogeneity is the misorientation of individual magnetic grains. This gives a horizontal component to the local magnetization, which may average out when integrated over the volume of the PM and thus not exhibit a dipole moment. However, the interaction of the horizontal moment of such a local dipole with the horizontal moment of its image produces a contribution to the vertical force. The vertical force of a dipole of moment m, oriented at angle θ to the vertical, with its diamagnetic image is

$$F_z=\frac{3\mu_0 m^2}{4\pi r^4}(2\cos^2\theta+\sin^2\theta), \quad (10)$$

whereas, if we measure the vertical magnetic moment as $m\cos\theta$ and calculate the force assuming the moment is purely vertical, we obtain

$$F_z=\frac{3\mu_0 m^2}{4\pi r^4}(2\cos^2\theta). \quad (11)$$

Clearly, the method of Eqs. (7)–(9) and associated assumptions will underestimate the force somewhat. A detailed examination of this effect, either experimentally or calculationally is beyond the scope of this article. However, we note that typical mean angular misorientations of grains in PMs such as the ones we are using are in the range of 20°–40°,[29,30] and this could easily account for the remaining discrepancy between theory and experiment in Fig. 10 for heights greater than 3 mm.

To calculate forces when the PM is moved horizontally, we must examine the situation when the current loops are not coaxial. To calculate the forces between two current loops, we use the method of Kim *et al.*[31] (corrected for typographi-

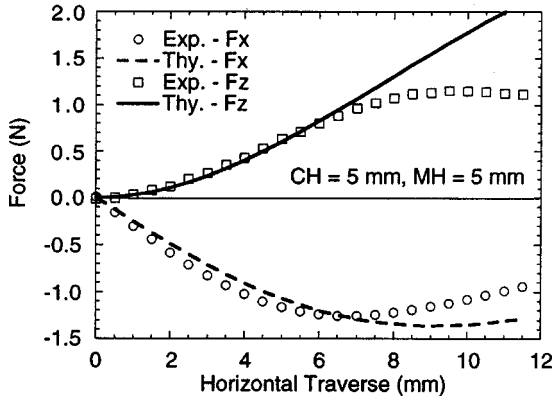

FIG. 11. Comparison of theoretical calculations with experimental values of vertical and horizontal forces vs horizontal displacement for FC.

cal errors). Denoting the horizontal offset of the center of one coil from the center of another by x, we have the horizontal force given by

$$F_x(I_1,I_2,x,z) = \frac{\mu_0 I_1 I_2 R_2}{2\pi}\int_{-\pi/2}^{\pi/2}[F_s(r_1,x,z)-F_s(r_2,x,z)]d\phi, \quad (12)$$

where

$$F_s(r,x,z)=\left(\frac{R_1^2-r^2-z^2}{(R_1-r)^2+z^2}E[k(r)]+K[k(r)]\right)\times\frac{\cos\phi}{[(R_1+r)^2+z^2]^{1/2}}, \quad (13)$$

$$r_1=[(R_2\cos\phi+x)^2+(R_2\sin\phi)^2]^{1/2}, \quad (14)$$

$$r_2=[(R_2\cos\phi-x)^2+(R_2\sin\phi)^2]^{1/2}, \quad (15)$$

$$k(r)=\frac{4R_1 r}{(R_1+r)^2+z^2}, \quad (16)$$

and for positive x, the vertical force is given by

$$F_z(I_1,I_2,x,z)=\frac{\mu_0 I_1 I_2 R_2 z}{\pi}\int_0^{\pi/2}[F_u(r_1,x,z,\beta_1)-F_u(r_2,x,z,\beta_2)]d\phi, \quad (17)$$

where

$$F_u(r,x,z,\beta)=\left(\frac{R_1^2+r^2+z^2}{(R_1-r)^2+z^2}E[k(r)]-K[k(r)]\right)\times\frac{\cos(\phi+\beta)}{r[(R_1+r)^2+z^2]^{1/2}}, \quad (18)$$

$$\beta_1=-\tan^{-1}\left(\frac{R_2\sin\phi}{x+R_2\cos\phi}\right), \quad (19)$$

$$\beta_2=\tan^{-1}\left(\frac{R_2\sin\phi}{x-R_2\cos\phi}\right), \quad 0\leqslant\beta_2\leqslant\pi. \quad (20)$$

Comparison of theoretical calculations of the forces versus the experimental data for horizontal movement of the PM at a CH of 5 mm is shown in Fig. 11. Here, the agreement between theory and experiment is reasonable for horizontal displacements less than 5 mm. Beyond 5 mm, the theoretical calculation shows that the vertical force asymptotically approaches 3.05 N, which is the theoretical vertical force for the diamagnetic interaction at 5 mm, while the experimental results show lower values. In addition to hysteresis effects beginning to dominate, the deviation occurs because in the theoretical model we assume that the HTS is a semi-infinite plane, whereas beyond about 5 mm of horizontal movement in the experiment, edge effects begin to be significant. Similar edge effects are seen in Fig. 3 for CH=30 mm, MH=5 mm. The horizontal force is similarly affected by hysteresis and edge effects for displacements beyond 5 mm.

For ZFC and heights greater than 10 mm, calculations using the frozen-image model agree with the experimental data shown in Fig. 10 to within 10%. For ZFC and heights greater than 6 mm, the agreement is within 20%. For FC and height changes less than 2 mm, the agreement is within 17%. For FC and lateral displacements less than 2 mm, calculations using the frozen-image model agree with the experimental data shown in Fig. 11 to within 15% for horizontal forces and 11% for vertical forces. These percentages are considerably lower if the maximum achievable forces are used in the denominator in each case, and the agreement of the predictions with the data is reasonable given the limited characterization of the magnetization of the PM. For FC and small movements from the FC_0 point, the experimental forces exceed the model predictions by approximately the same amount. This is consistent with the agreement between the model and experiment to about 1% for the ratio of vertical to horizontal stiffness at FC_0, and it is consistent with the hypothesis that the permanent magnet contains regions with a horizontal component to the local magnetization.

V. CONCLUSIONS

We analyzed the forces and associated stiffnesses theoretically and experimentally for a PM/HTS system in ZFC, FC, and at FC_0. We derived the interaction forces and respective stiffnesses by the frozen-image method and compared with the experimental results. Experimental results and the model were in reasonable agreement for vertical or horizontal displacements within several mm of the field-cooling position and is probably sufficiently accurate for calculating levitation forces and stiffnesses in most practical applications.

Experiments showed that the forces and associated stiffnesses were strongly dependent on the cooling history with a low hysteresis. For high CHs (ZFC), the interaction between the PM/HTS system is described as diamagnetic, while for low CHs (FC), the diamagnetic behavior is accompanied by large flux pinning. Higher hysteresis was observed in lateral forces than in vertical forces during lateral traverses. This may be attributed to movement of flux lines that are mostly in a lateral rather than vertical direction. Cross stiffness (change in vertical force) was observed during lateral movements. During spindown experiments, the coefficient of friction was double valued, a result predicted in a theory by Sugiura *et al.*[19] where cross stiffness is present. Vertical

stiffness was approximately independent of descent versus ascent, but on closer inspection, a slight difference was observed and was attributed to different amounts of trapped flux in the HTS during a particular vertical traverse.

In ZFC, because the interaction between the PM and HTS is almost diamagnetic, there is high vertical stiffness and no lateral stiffness. In addition, vertical stiffness is higher in ZFC than in FC_0 and was twice the lateral stiffness for each CH. These results were predicted by the frozen-image model. The model also predicted that the cross stiffness K_{zx} is zero at $x=0$ and decreases with increasing CH. In addition, the frozen-image model successfully predicted qualitatively the general behavior of the forces and stiffnesses; however, for larger movements of the PM, agreement with the experiments was lower because the experimental results were strongly influenced by irreversible magnetization and edge effects.

ACKNOWLEDGMENTS

This work was partially supported by the U. S. Department of Energy, under Contract No. W-31-109-Eng-38. One of the authors (A.C.) gratefully acknowledges the support of the Turkish government. The authors are indebted to B. Veal of Argonne and to Nippon Steel for providing the samples used in these experiments, and to T. Mulcahy and K. Uherka of ANL for commenting on an early draft of the manuscript.

[1] J. R. Hull, T. M. Mulcahy, K. L. Uherka, R. A. Erck, and R. G. Abboud, Appl. Supercond. **2**, 449 (1994).
[2] Q. Y. Chen, Z. Xia, K. B. Ma, C. K. McMichael, M. Lamb, R. S. Cooley, P. C. Fowler, and W. K. Chu, Appl. Supercond. **2**, 457 (1994).
[3] H. J. Borneman, A. Tonoli, T. Ritter, C. Urban, O. Zaitsev, K. Weber, and H. Reischel, IEEE Trans. Appl. Supercond. **5**, 618 (1995).
[4] R. Takahata, H. Ueyama, Y. Miyagawa, H. Kameno, H. Higasa, and H. Ishikawa, *5th International Symposium on Magnetic Bearings*, Japan, 1996.
[5] F. C. Moon and P.-Z. Chang, Appl. Phys. Lett. **56**, 397 (1990).
[6] B. R. Weinberger, L. Lynds, J. Van Valzah, H. E. Eaton, J. R. Hull, T. M. Mulcahy, and S. A. Basinger, IEEE Trans. Magn. **27**, 2415 (1991).
[7] J. R. Hull, E. F. Hilton, T. M. Mulcahy, Z. J. Yang, A. Lockwood, and M. Strasik, J. Appl. Phys. **78**, 6833 (1995).
[8] E. H. Brandt, Appl. Phys. Lett. **53**, 1554 (1988); Am. J. Phys. **58**, 43 (1990).
[9] F. C. Moon, M. M. Yanoviak, and R. Ware, Appl. Phys. Lett. **52**, 1534 (1988).
[10] F. C. Moon, K.-C. Weng, and P.-Z. Chang, J. Appl. Phys. **66**, 5643 (1989).
[11] L. C. Davis, J. Appl. Phys. **67**, 2631 (1990).
[12] T. H. Johansen and H. Bratsberg, J. Appl. Phys. **74**, 4060 (1993).
[13] A. B. Riise, T. H. Johansen, and H. Bratsberg, Physica C **234**, 108 (1994).
[14] A. Sanchez and C. Navau, Physica C **268**, 46 (1996).
[15] T. Hikihara and F. C. Moon, Physica C **250**, 121 (1995).
[16] A. N. Terentiev and A. A. Kuzunetsov, Physica C **195**, 41 (1992).
[17] T. Sugiura and H. Fujimori, IEEE Trans. Magn. **32**, 1066 (1996).
[18] T. Sugiura, K. Matsunaga, Y. Uematsu, T. Aoyagi, and M. Yoshizawa, *Proceedings of the 10th International Symposium on Superconductivity*, Gifu, Japan, October 1997, pp. 1349–1352.
[19] A. A. Kordyuk, J. Appl. Phys. **83**, 610 (1998).
[20] K.-D. Durst and H. Kronmuller, J. Magn. Magn. Mater. **68**, 63 (1987).
[21] Ugimag, Inc. (1996) (unpublished).
[22] B. R. Weinberger, L. Lynds, and J. R. Hull, Supercond. Sci. Technol. **3**, 381 (1990).
[23] P.-Z. Chang, F. C. Moon, J. R. Hull, and T. M. Mulcahy, J. Appl. Phys. **67**, 4358 (1990).
[24] J. R. Hull, T. M Mulcahy, K. Salama, V. Selvamanickam, B. R. Weinberger, and L. Lynds, J. Appl. Phys. **72**, 2089 (1992).
[25] F. C. Moon, J. Appl. Electromagn. Mat **1**, 29 (1990).
[26] C. Navau and A. Sanchez, Phys. Rev. B **58**, 963 (1998).
[27] M. Abramowitz and I. A. Stegun, *Handbook of Mathematical Functions*, NBS Applied Mathematics Series **55** (1964).
[28] F. C. Moon, *Magnetosolid Mechanics* (Wiley, New York, 1984), p. 421.
[29] O. B. G. Assis, V. Sinka, and M. Ferrante, J. Mater. Sci. Lett. **13**, 1141 (1994).
[30] A. S. Kim, F. E. Camp, and H. H. Stadelmaier, J. Appl. Phys. **76**, 6265 (1994).
[31] K.-B. Kim, E. Levi, Z. Zabar, and L. Birenbaum, IEEE Trans. Magn. **32**, 478 (1996).